© American Society for Mass Spectrometry, 2016

J. Am. Soc. Mass Spectrom. (2016) 27:1694–1702
DOI: 10.1007/s13361-016-1439-4

RESEARCH ARTICLE

$Si_{1-x}Ge_x$/Si Interface Profiles Measured to Sub-Nanometer Precision Using uleSIMS Energy Sequencing

R. J. H. Morris,[1,2] T. P. A. Hase,[1] A. M. Sanchez,[1] G. Rowlands[1]

[1]University of Warwick, Gibbet Hill Road, Coventry, CV4 7AL, UK
[2]IMEC, Kapeldreef 75, B-3001, Leuven, Belgium

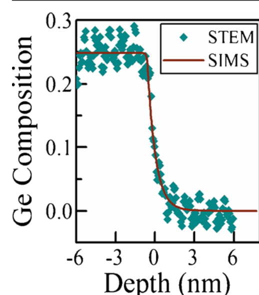

Abstract. The utility of energy sequencing for extracting an accurate matrix level interface profile using ultra-low energy SIMS (uleSIMS) is reported. Normally incident O_2^+ over an energy range of 0.25–2.5 keV were used to probe the interface between $Si_{0.73}Ge_{0.27}$/Si, which was also studied using high angle annular dark field scanning transmission electron microscopy (HAADF-STEM). All the SIMS profiles were linearized by taking the well understood matrix effects on ion yield and erosion rate into account. A method based on simultaneous fitting of the SIMS profiles measured at different energies is presented, which allows the intrinsic sample profile to be determined to sub-nanometer precision. Excellent agreement was found between the directly imaged HAADF-STEM interface and that derived from SIMS.

Keywords: SIMS, Si/$Si_{1-x}Ge_x$, Ultra low energy depth profiling

Received: 26 February 2016/Revised: 27 May 2016/Accepted: 17 June 2016/Published Online: 21 July 2016

Introduction

With the advancement of growth technologies such as chemical vapour deposition (CVD), atomic layer deposition (ALD), molecular beam epitaxy (MBE), pulsed laser deposition (PLD) etc., devices are now routinely composed of many different layers. These layers may range from only a few atomic planes up to many microns, forming complex tailored heterostructures to meet a large and diverse range of technological applications. Device parameters are often controlled through direct modification of the electronic band structure through choice of crystal structure and material. Additional tailoring is, however, possible through varying the layer thickness, composition, and dopant. Critical to the device functionality and its subsequent exploitation is the quality of the buried interfaces because these can influence the overall performance [1]. To meet the semiconductor technology roadmap [2], heterostructures have continually decreased in size with concomitant increases in their complexity. As we approach the resolution limit of certain characterization techniques, obtaining an accurate picture of the sample structure is becoming extremely challenging.

Secondary ion mass spectrometry (SIMS) is an essential characterization technique that has been exploited by the semiconductor industry over several decades. SIMS offers numerous advantages over other characterization techniques such as scanning and transmission electron microscopy (SEM/TEM) and X-ray diffraction (XRD). It enables a quantitative and precise determination of the matrix and dopant concentrations as a function of depth to be obtained. Such functionality has meant that SIMS has become the technique of choice for concentration measurements across many academic and industrial sectors. Over the years, there has been a significant amount of research and models developed to ensure that SIMS can quantify accurately layer thicknesses and composition of doping layers (including δ-doping) in the latest quantum-well structures [3]. However, with the drive to further optimize device performance, there is increasing emphasis on interfaces, and SIMS metrology needs to be extended to facilitate accurate analysis of layered systems and their interfaces.

Unfortunately, current SIMS analysis of interfaces is hampered by the probe–sample interaction, which modifies the interface profile shape. The depth resolution achievable in SIMS profiling is dependent on a number of factors, including the flatness of the initial surface and the use of measurement conditions, which do not introduce surface topography through ion-beam roughening. Even under the most favorable experimental conditions, there will still exist some atomic mixing induced by the interaction of the incident ions with the sample matrix [4]. The highest obtainable SIMS resolution, therefore, occurs as the primary beam energy, E_P, tends towards zero [i.e.,

Correspondence to: R. J. H. Morris; *e-mail:* r.morris@warwick.ac.uk

ultra-low energy SIMS (uleSIMS)]. However, there are physical limitations as to how low E_P can be reduced to, and Clegg [5] proposed energy sequencing as a potential way of synthesizing the "zero energy" profile. The method involves obtaining profiles from the same sample at several different beam energies and extrapolating the fitted profile to zero energy, thereby removing the ion beam energy-induced structural modifications. Previous studies employing such an energy sequencing method have involved profiling buried layers within a single matrix material (e.g., boron δ-layers in silicon [6] and Si or Al δ-layers in GaAs [7]). By concentrating on buried δ-layers, and not interfaces, these studies avoided any complications associated from the matrix [8, 9] and transient effects [10], as well as the need to develop suitable models to describe the spatial extent of an interface.

In this paper, we extend the metrology of energy sequencing protocols and show how it can be applied to the technologically important $Si/Si_{1-x}Ge_x$ system to extract interface profiles using SIMS with sub-nanometer precision. Through comparison of the interface profile determined from SIMS with that obtained using high angle annular dark field scanning transmission electron microscopy (HAADF-STEM), the SIMS metrology is benchmarked against a traceable measurement when combined with XRD.

Experimental

A superficial $Si_{0.73}Ge_{0.27}$ layer of nominal 27 nm thickness was deposited onto a prepared Si (100) wafer using CVD. The Ge composition and crystalline parameters were determined from high resolution XRD. Prior to any SIMS measurements, the sample surface was cleaned in a dilute (5%) HF solution until its wetting properties indicated a hydrophobic surface. This implied any particulate contamination, which would otherwise degrade the SIMS results, had been removed. To prevent further surface contamination, all the SIMS profiles were carried out without breaking the ultra-high vacuum.

The SIMS depth profiling was performed using an Atomika 4500 instrument, a primary O_2^+ beam at near normal incidence with energies in the 0.25–2.5 keV range. A scan area of 220 × 220 μm was used with a linear gate size of 6.25% applied to the collected data. This procedure was adopted for all the profiles such that data could be compared from the flat crater bottom region, which measured only 13.8 × 13.8 μm and, thereby, avoided any edge effects that can be more pronounced at low beam energies. Previous studies under these conditions showed profiling without any additional artefacts introduced through surface topological changes [11]. Optical conductivity enhancement (OCE) [12] in the form of red laser illumination (λ = 635 nm: power = 2.5 mW: spot size ~2 mm at the sample) was used to stabilize the sample surface bias as the material was intrinsic (i.e., highly resistive). Following depth profiling, all craters were measured using a calibrated Dektak (Santa Barbara, California, US) 3030 stylus profilometer. The depth of each crater was averaged three times across different lateral regions with the spread in measurement ≤ ±3%.

In order to demonstrate the degree of surface flatness, atomic force microscopy (AFM) measurements on the virgin and all crater surfaces were performed using a Veeco (New York, US) multimode AFM system with a Nanoscope 3A controller. These measurements were made in contact mode over a 5 × 5 μm area using a scan rate of 1 Hz. For the virgin sample surface and in each SIMS crater, three measurements from different regions were taken. In all cases, the roughness values deduced from the repeat scans were within experimental uncertainty.

Transmission electron microscopy (TEM) imaging of the sample was carried out using a JEOL 2000FX microscope operating at 200 kV. High angle annular dark field-scanning transmission electron microscopy (HAADF-STEM) imaging of the $Si_{0.73}Ge_{0.27}/Si$ interface was done using a spherical aberration corrected JEOL (Tokyo, Japan) 2100F microscope, also operating at 200 kV.

Results

Microscopy

Figure 1a shows the TEM cross section image of the virgin $Si_{0.73}Ge_{0.27}/Si$ layers. The layer quality is excellent with a smooth interface without any evidence of misfit or threading dislocations. The sample surface also appears to show no significant roughness. AFM of a 5 × 5 μm area of the sample surface is shown in Figure 1b. The scan appears almost featureless, in agreement with the observed low roughness seen in the HRTEM. The surface roughness determined from the AFM was close to its resolution limit and was 0.10 ± 0.10 nm with few, if any, terraces associated with any miss-cut of the Si wafer (<0.1°) being observed.

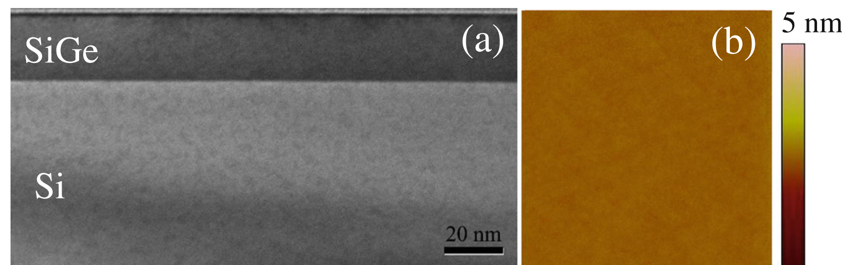

Figure 1. (a) High resolution transmission electron microscopy image of the $Si_{0.73}Ge_{0.27}$ layer on Si. The (004) crystalline direction is normal to the surface; **(b)** a 5 × 5 μm AFM image of the virgin $Si_{0.73}Ge_{27}$ sample surface showing no discernible features

HAADF-STEM imaging of the interface between the Si and $Si_{0.73}Ge_{0.27}$ layers was used to obtain an interface profile with atomic resolution. HAADF-STEM imaging is highly sensitive to the atomic number Z of the scattering species and therefore offers a direct high resolution image of the atomic distribution [13]. HAADF-STEM images are also referred to as Z-contrast images [14] because the flux scattered onto the detector has been found to scale as $Z^{1.7}$. For a random $Si_{1-x}Ge_x$ alloy compared to Si of the same thickness, the ratio of the scattered intensity scales by a factor G given by:

$$G = \frac{I_{Si_{1-x}Ge_x}}{I_{Si}} = \left(\frac{9x}{7}+1\right)^{1.7}. \quad (1)$$

Here, $I_{Si_{1-x}Ge_x}$ and I_{Si} are the measured intensities from the $Si_{1-x}Ge_x$ and Si regions, and x the Ge fraction. Figure 2a shows the HAADF-STEM image taken from the interface region where columns of highly ordered atoms are observed. From this image, the interface is estimated to span ~5 unit cells. The Ge concentration as a function of position was determined using Equation 1 and within the bulk $Si_{1-x}Ge_x$ layer found to be $x \sim 0.27$, in excellent agreement with XRD and independent SIMS analysis. The spatial variation of the composition across the interface is shown in Figure 2b. The high atomic resolution introduces fluctuations into the intensity profile as the atomic columns are aliased. This adds uncertainty to the line scan profile, and, to obtain a quantifiable fit to the profile, the line scan was spatially averaged.

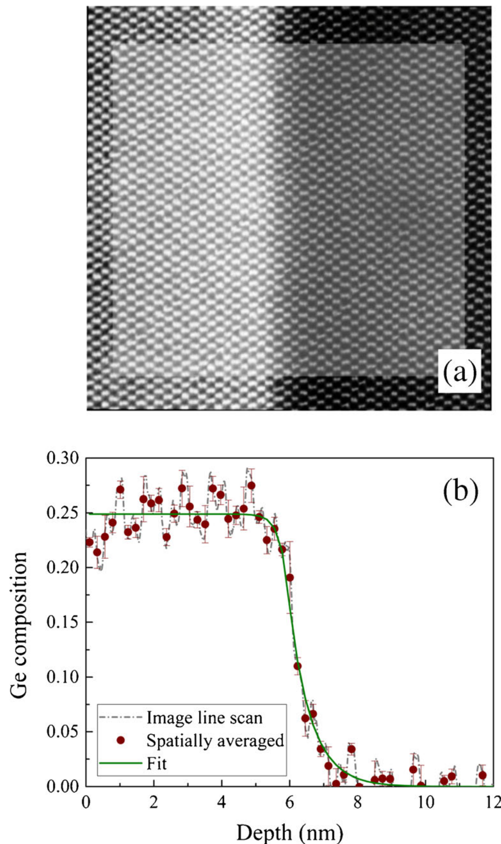

Figure 2. (Color on-line) **(a)** HAADF-STEM image of the $Si_{0.73}Ge_{0.27}$/Si interface region showing the atomic columns; **(b)** line scan across the interface showing the Ge concentration perpendicular to the interface as a function of position (nm). Fit to spatially averaged data obtained using Equation 2

Various analytic models exist with which to parameterize a given interface, which can be symmetric or asymmetric depending on the chosen function. In this paper, we have chosen to parameterize the interface using a profile function, F_{Sample}, based on two exponentials:

$$F_{sample}(z) = \begin{cases} \alpha \exp\left({}^{(z-z_0)}\Big/_{s_u}\right) & for\ z \le z_0 \\ 1-\left[(1-\alpha)\exp\left(-{}^{(z-z_0)}\Big/_{s_d}\right)\right] & for\ z > z_0 \end{cases}. \quad (2)$$

Here $\alpha = {}^{s_u}/_{(s_u+s_d)}$ ensures the function is normalized and is continuous at the cross-over position, z_0, when the interface is asymmetric (i.e., $s_u \neq s_d$). The interface position is defined using the expectation value (center-of-mass) whose position, $\bar{z}$, is given by:

$$\bar{z} = z_0 + (s_d - s_u). \quad (3)$$

The advantage of this particular function is its relative simplicity, and it can be used to describe a wide range of interface profiles, with s_u and s_d defining the widths of the upper (s_u) and lower (s_d) parts of the interface. The function even approximates interfaces defined by the symmetric ($s_u = s_d$) error function satisfactorily. More importantly, the experimental HAADF-STEM profile is well fitted to the proposed interface model (Equation 2) as shown in Figure 2b, where we have fitted $(1 - F_{sample})$ because of our layer order. The model is simply scaled by the Ge concentration well away from the interface. Owing to the fluctuations introduced by the aliasing of the atomic columns in the HAADF-STEM image, the uncertainties in the fitted parameters are relatively large. We find z_0 to occur at a concentration of $x = 0.18 \pm 0.03$ with $s_u = 0.2 \pm 0.1$ nm, and $s_d = 0.6 \pm 0.3$ nm. The position of the interface, $\bar{z}$, occurs at a composition of $x \simeq 0.1$.

SIMS

The same sample was then subject to a detailed SIMS analysis. Post SIMS, all the resulting craters were analyzed using AFM (not shown). As for the virgin surface, the crater bottoms were found to be extremely flat and almost featureless. Table 1 summarizes the RMS roughness obtained from the AFM. The similarity between craters of different E_P suggests that the probe–sample interaction for this energy range did not degrade the sample topography during the profiling [11]. Owing to the importance of $Si_{1-x}Ge_x$ in modern transistor technologies [15], this material system has been studied widely using SIMS. Hence, the profile quantification was carried out using

Table 1. RMS Roughness Analysis from AFM Images of the Sample Surface and Various SIMS Beam Energy Craters

Analysis area (5 × 5) μm	RMS roughness (nm)
Virgin surface	0.10 ± 0.1
250 eV crater	0.08 ± 0.1
500 eV crater	0.08 ± 0.1
1.0 keV crater	0.08 ± 0.1
1.5 keV crater	0.08 ± 0.1
2.0 keV crater	0.08 ± 0.1
2.5 keV crater	0.09 ± 0.1

previously developed metrologies [3, 11] for both the Ge concentration and erosion rate ($\dot{z}$): the mean Ge^+ yield from the layer was converted to the concentration established from previous XRD analysis. As the measured Ge^+ yield had previously been shown to vary proportionally with x over the limited concentration range of the sample (i.e., $0 \leq x \leq 0.3$ [11, 16]), no further correction was needed. Moreover, from the measured SIMS depth profiles there was no indication of any transient behavior as we profile through the interface, unlike at the surface. This is believed to be because at near normal incidence and once steady state profiling is reached, the amount of oxygen present is more than sufficient to fully oxidize both the Si and Ge present [17]. Given that the free energy of formation for SiO_2 and GeO_2 is 825.9 and 491.3 kJ/mol, respectively [18], it is clear that Si will preferentially oxidize. Thus, if the oxygen level were too low for full oxidation to occur, metallic Ge will segregate out of the growing intermixed oxide layers. For higher incidence angle (30°–60°) analysis of SiGe, this has been observed [19, 20] but we find no evidence for it in our experimental data. To convert the profile time (min) into a depth z (nm), a slightly more complicated approach was required. Over this range of x, the erosion rate, $\dot{z}$, is known to increase monotonically with x and is well described by the function [11]:

$$\dot{z} = U + V\exp\left({}^{x}/_{W}\right), \tag{4}$$

where x is the Ge concentration and U, V, and W constants with values 0.77, 0.23, and 48.10, respectively. Having already established the Ge concentration from XRD, a point by point erosion rate correction (using Equation 4) to rescale the linear time axis taking into account the erosion rate variation with matrix was used. This results in a nonlinear stretched time axis, and this newly scaled time axis is then converted to depth using the measured crater depth value. This process is illustrated in Figure 3; Figure 3a shows the raw SIMS profiles (i.e., Ge^+ yield as a function of time) for each primary beam energy from which no evidence of any interface transient behavior is observed. Figure 3b shows the 500 eV depth profile only and following the concentration calibration step, whereas Figure 3c shows the same profile after the time axis has be converted to depth.

Any data obtained from a SIMS experiment will be a convolution of two functions; the first, $R(E, z)$, describes the energy-dependent interaction of the ion beam with the sample (commonly referred to as the SIMS response function), whilst the second describes the intrinsic sample feature being probed, $F_{Sample}(z)$. If $F_{Sample}(z)$ is known, or can be approximated to a simple analytical function, as in the case of a δ-layer, then the response function for the given measurement conditions can be determined. Such an approach has been used in previous studies exploiting boron δ-layers in Si, which have been used to determine a generic SIMS response function capturing the

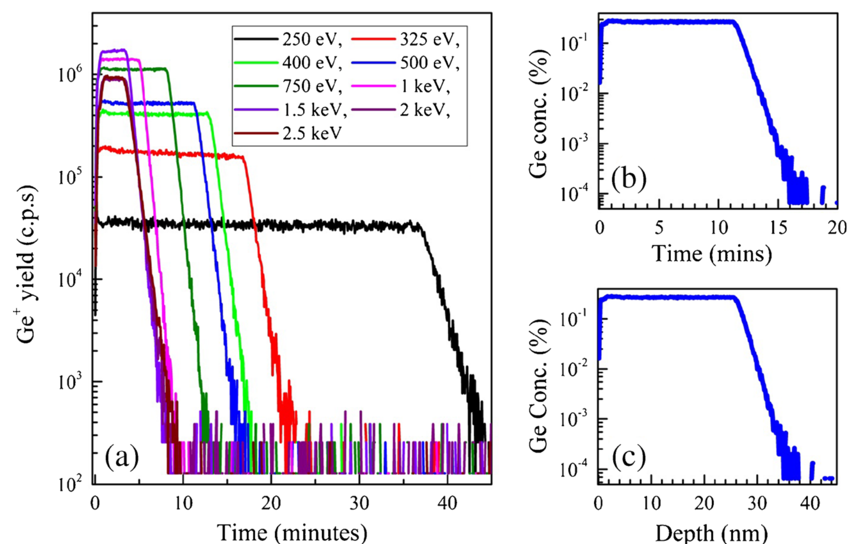

Figure 3. (Color on-line) **(a)** All the as-measured SIMS depth profiles; **(b)** the 500 eV SIMS depth profile after concentration quantification using the previously found XRD value for the Ge concentration ($x \sim 0.27$); **(c)** the same 500 eV SIMS depth profile after depth calibration using a point by point erosion rate correction and Equation 4

essential ion–sample interactions [21]. Conversely, if $R(E,z)$ were known precisely, then $F_{Sample}(z)$ could be obtained from a single SIMS profile by calculating explicitly the convolution $R(E,z) \otimes F_{Sample}(z)$ for different models of the sample profile.

However, in the more general case, and as described herein, both $R(E,z)$ and $F_{Sample}(z)$ are unknown: the response function depends on the exact matrix (sample) as well as the specific instrumental parameters used and the sample profile is what is to be determined. As $R(E,z)$ is energy-dependent, the blurring of the sample features introduced by the ion beam interactions is significantly reduced at low energies. In the limit where $E_P \rightarrow 0$, the SIMS response function, $R(E,z) \rightarrow \delta_z$ and the SIMS measures $F_{Sample}(z)$ directly. However, achieving the E_P required to sufficiently minimize the atomic mixing and resolve the interface within a single SIMS measurement may well be beyond current technological limits. Hence, new metrologies are required to extract $F_{Sample}(z)$ and mitigate the effect of the ion–sample interactions. Below, we describe a simplified method to model the energy-dependent changes in $R(E,z)$ and allow $F_{Sample}(z)$ to be quantified.

The approach adopted presumes a simplistic model to parameterize the SIMS response, $R(E,z)$, and assumes that the interface can be modeled using the analytical expression given in Equation 2. The first step is to define a parameterizable SIMS response function. As a first approximation, and to help simplify the convolution, a double exponential function as given by:

$$R(E,z) = \begin{cases} \beta \exp\left({}^{z}/_{\rho_u(E_P)} \right) & for \;\; z \leq 0 \\ \beta \exp\left({}^{-z}/_{\rho_d(E_P)} \right) & for \;\; z > 0 \end{cases}, \qquad (5)$$

was adopted where $\rho_d(E_P) > \rho_u(E_P)$. Here the pre-factor β is a renormalization term ensuring that $\int_{\infty}^{-\infty} R(E,z) = 1$ and is related to the $\rho_{u/d}(E_P)$ parameters through $\beta^{-1} \equiv (\rho_u(E_P) + \rho_d(E_P))$. The $\rho_{u/d}$ parameters are not linked directly to any physical ion–sample interactions. Broadly, however, $\rho_d(E_P)$ will be related to the depth of the ion induced distribution within the altered layer and the surface escape probability whilst $\rho_u(E_P)$ is related to the depth of any surface features, including effects such as surface roughening due to ion bombardment and the effective escape depth [21]. It is expected that $\rho_u(E_P)$ is small and tends towards 0. This simple approximation, which captures the general features of a SIMS response function with depth, is, however, clearly not physical as it is cusped at $z = 0$, but it does allow an analytic expression for the convolution $R(E,z) \otimes F_{Sample}(z)$ to be determined analytically.

The convolution of $R(E,z) \otimes F_{Sample}(z)$ was determined using a sum of multiple integrals due to the fact that the derivatives of $R(E,z)$ and $F_{Sample}(z)$ are not continuous. We reproduce the derivation below for completeness but the result of the convolution is given in Equation 7.

The integrals are performed over the dummy variable y:

$$R(E,z) \otimes F_{Sample}(z) = \begin{cases} \int_{-\infty}^{z'} U1 \; dy + \int_{z'}^{0} U2 \; dy + \int_{0}^{\infty} U3 \; dy & for \;\; z' \leq 0 \\ \int_{-\infty}^{0} D1 \; dy + \int_{0}^{z'} D2 \; dy + \int_{z'}^{\infty} D3 \; dy & for \;\; z' > 0 \end{cases}, \qquad (6)$$

with

$$U1 = \beta \exp\left({}^{y}/_{\rho_u} \right) \left[1 - (1-\alpha) \exp\left(- {}^{(z'-y)}/_{s_d} \right) \right],$$

$$U2 = \alpha\beta \exp\left({}^{y}/_{\rho_u} \right) \exp\left({}^{(z'-y)}/_{s_u} \right)$$

and $U3 = \alpha\beta \exp\left({}^{-y}/_{\rho_d} \right) \exp\left({}^{(z'-y)}/_{s_u} \right)$.

Similarly, the integrands for $z' > 0$ are given by; $D1 = \beta \exp\left({}^{y}/_{\rho_u} \right) \left[1 - (1-\alpha) \exp\left(- {}^{(z'-y)}/_{s_d} \right) \right]$, $D2 = \beta \exp\left({}^{-y}/_{\rho_d} \right) \left[1 - (1-\alpha) \exp\left(- {}^{(z'-y)}/_{s_d} \right) \right]$ and $D3 = \alpha\beta \exp\left({}^{-y}/_{\rho_d} \right) \exp\left({}^{(z'-y)}/_{s_u} \right)$.

Here, $z' = z - z_0$ with z_0 being the cross-over point of $F_{sample}(z)$.

The convolution of our simple SIMS response function (Equation 5) and the interface parameterized by Equation 2 is found to be the relatively simple sum of two exponentials either side of the cross-over point, z', given by:

$$R(E,z) \otimes F_{Sample}(z) = \begin{cases} A \exp\left({}^{z'}/_{\rho_u} \right) + B \exp\left({}^{z'}/_{s_u} \right) & for \;\; Z' \leq 0 \\ A' \exp\left(- {}^{z'}/_{\rho_d} \right) + B' \exp\left(- {}^{z'}/_{s_d} \right) + 1 & for \;\; Z' > 0 \end{cases}, \qquad (7)$$

with the coefficients A, A', B, and B' all being functions of ρ_u, ρ_d, s_u and s_d given by:

$$A = \frac{\rho_u^3}{(\rho_u - s_u)(s_d + \rho_u)(\rho_d + \rho_u)}$$

$$B = \frac{-s_u^3}{(\rho_u - s_u)(\rho_d + s_u)(s_u + s_d)}, \qquad (8)$$

and

$$A' = \frac{-\rho_d^3}{(\rho_d - s_d)(\rho_d + s_u)(\rho_d + \rho_u)}$$

$$B' = \frac{s_d^3}{(\rho_d - s_d)(s_d + \rho_u)(s_u + s_d)}. \qquad (9)$$

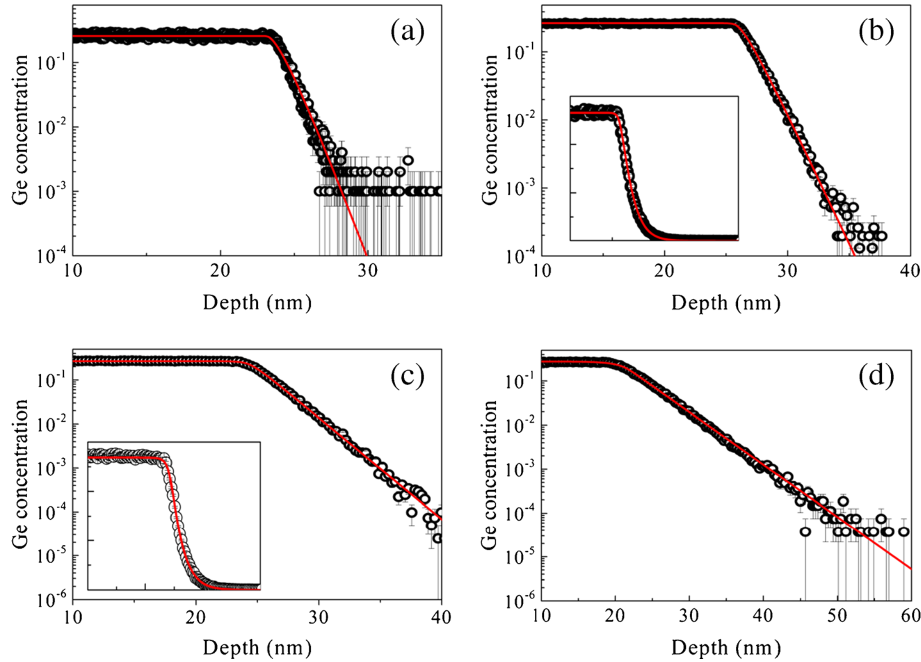

Figure 4. Selection of SIMS profiles (points) and their fits (lines) based on Equation 7, **(a)** 250 eV, **(b)** 500 eV, **(c)** 1 keV, and **(d)** 2.5 keV. Inserts in **(b)** and **(c)** show the same data but on a linear–linear scale demonstrating the quality of the fit over the entire concentration range

The center of mass of the convolved function, $\overline{\zeta}$, is located at:

$$\overline{\zeta} = z_0 + \left(\rho_u A + s_u B + \rho_d A' + s_d B'\right). \quad (10)$$

From Equation 7 it can be seen that any measured SIMS profile will depend on all the sample and SIMS parameters (i.e., s_u, s_d, ρ_u, and ρ_d). Thus, it is not possible, from a single measurement, to separate s_u and s_d from the energy-dependant $\rho_{u/d}$ terms. Nor is it possible to fit the individual SIMS profiles to some function and exploit energy sequencing to separate s_u and s_d directly [22]. Therefore, further simplification and a slightly different approach are required.

The fitting can be facilitated further by modeling the energy-dependent response function terms $\rho_{u/d}$ as simple power laws of the form [20, 23, 24]:

$$\rho_{u/d}(E_P) = k_{u/d} \cdot E_P^{n_{u/d}}. \quad (11)$$

Table 2. Global Best Fit Parameters from Fitting All the Measured SIMS Profiles with Energy in keV

Fit parameters	
s_u	0.07±0.10 nm
s_d	0.62±0.05 nm
k_u	0.63±0.05 nm
n_u	1.24±0.11
k_d	1.883±0.011 nm
n_d	0.720±0.009

Again, there is no physical justification underpinning Equation 11 with the variables $k_{u/d}$ and $n_{u/d}$ simply parameterizing the energy dependence of $\rho_{u/d}$ and assumes the energy behavior is continuous and can be extrapolated to zero. However, to fully exploit Equation 11, the data *set* of the SIMS profiles recorded for all the different energies now needs to be fitted simultaneously. The global input parameters for a simultaneous fitting approach include the following: the sample parameters

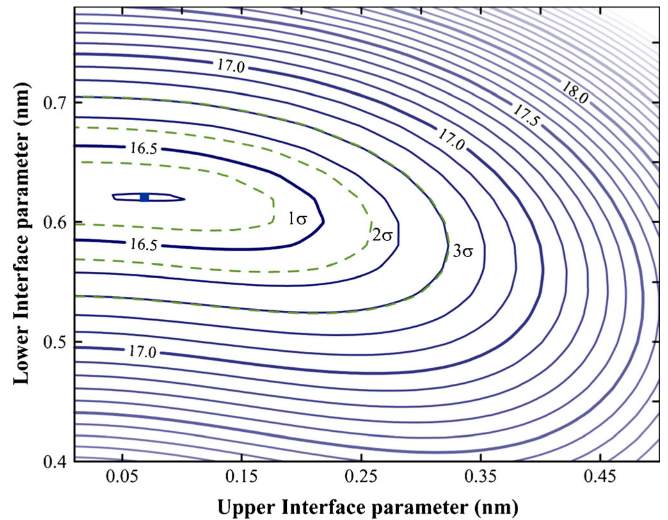

Figure 5. (Color on-line) Error surface showing the variation of the goodness-of-fit parameter as a function of s_d and s_u. For each set of $s_{d/u}$ values, all other fit parameters were minimized. The solid point marks the best fit parameters with the goodness-of-fit, $\chi_v^2 = 16.438$. The dashed lines show the 1σ, 2σ, and 3σ uncertainty contours, which are unbounded for s_u due to the constraint that $s_u \geq 0.01$ applied in the fitting procedure

$s_{u/d}$, (with an arbitrary constraint being $s_u \geq 0.01$ nm) and the four variables $k_{u/d}$ and $n_{u/d}$, which parameterize $\rho_{u/d}(E)$ for each energy. These six parameters ($s_{u/d}$, $k_{u/d}$, and $n_{u/d}$) mean that a minimum of seven energy profiles are required to refine and determine error bars on the fit parameters. Additionally, fitting of the cross-over point, z_0, along with a further refinement on the Ge concentration well inside the SiGe region were also performed for each profile. Again, due to the layer ordering of our sample the SIMS data were fitted to $R(E,z) \otimes (1 - F_{Sample}(z)) \equiv 1 - (R(E,z) \otimes F_{Sample}(z))$ using a Marquardt-Levenberg minimization of χ^2. As the number of data points in each SIMS profile varied, the simultaneous fit minimized a global goodness-of-fit parameter, which was the sum of the individual reduced χ^2 from each profile [25]. This methodology ensured each profile was weighted equally in the global fit. By using the experimental uncertainties on each data point, which arise predominantly from Poisson counting statistics, we are able to exploit the χ^2 probability distribution function in our analysis. Thus, the error bar quoted on each fitted variable is the 68% confidence interval [25].

In the global simultaneous fit, each profile is fitted to Equation 7. As the $s_{u/d}$ parameters are energy-independent, they are shared across all the energy profiles and are a shared or global fit parameter. On the other hand, the $\rho_{u/d}$ parameters for each energy are necessarily different and calculated using Equation 11 for each energy. $\rho_{u/d}$ are thus recalculated as the global variables $k_{u/d}$ and $n_{u/d}$ are refined during the fit. Figure 4 shows the 0.25, 0.5, 1, and 2.5 keV SIMS profiles along with their respective fits. As can be seen in the figure, a good fit to each profile was obtained, with a similar quality of fit ($\chi_v^2 \simeq 1.8$) being found for the other E_P profiles (not shown). The best-fit parameters from the fit to all the data are summarized in Table 2, but the sample parameters were found to be $s_u = 0.07 \pm 0.10$ nm and $s_d = 0.62 \pm 0.03$ nm showing excellent agreement with the previously fitted HAADF-STEM data. The relatively noisy data for low ion energies does, however, limit the precision of s_u with the goodness-of-fit error surface (Figure 5) only showing a poorly defined minimum for this parameter. Conversely, the s_d parameter is much better defined, as evidenced by the deep and clear minimum in the error surface.

Figure 6a shows the HAADF-STEM line scan and F_{sample} determined independently from the fitting of the energy sequencing SIMS. The profiles are rescaled on the horizontal axis to $z-\bar{\zeta}$, but there is no rescaling on the vertical axes. The interface profile derived from the SIMS analysis is an excellent representation of the atomically resolved interface. The composition at $\bar{\zeta}$ determined from the global SIMS fit was $x = 0.108(5)$, again in excellent agreement with the HAADF-STEM data. Figure 6b shows the evolution of the measured SIMS profiles as a function of energy, again with the depth axis rescaled to $z-\bar{\zeta}$ (with $\bar{\zeta}$ determined from the fits), which then allows a direct comparison between the data. It is clear that the SIMS profiles taken above 1 keV are not in good agreement with the interface profile determined from HAADF-STEM, but as E_p is lowered, the agreement between the two techniques improves as the effect of the ion mixing is reduced. From Equation 7 and Table 2 it is also clear that the broadening of the interface is dominated by the energy dependence of ρ_d, which enters into each of the coefficients A, A', B, and B'. This causes both the upper and lower parts of the interface to be broadened and is, perhaps, not unsurprising because this is the term related to the ion-induced distribution within the altered layer. Any SIMS measurement will, therefore, always be broadened (Figure 6b). In the past, the degree of broadening has sometimes been used as a proxy for the "resolution" of the measurement but this approach is limited because it assumes the interface to be perfectly sharp (i.e., a Heaviside function), and often uses statistical tests that are only weakly related to realistic SIMS response functions [26]. The approach highlighted herein is able to overcome this "resolution" limitation and extracts robust values of $s_{u/d}$ and their uncertainties because the interdependency of the convolved sample parameters are refined with each *energy change* within the global fit. Even by excluding the lowest energy (250 eV) from our simultaneous fit yields sample parameters of $s_u = 0.01 \pm 0.16$ nm and $s_d = 0.65 \pm 0.03$ nm, still in good agreement with the HAADF-STEM and consistent with the values determined from all the

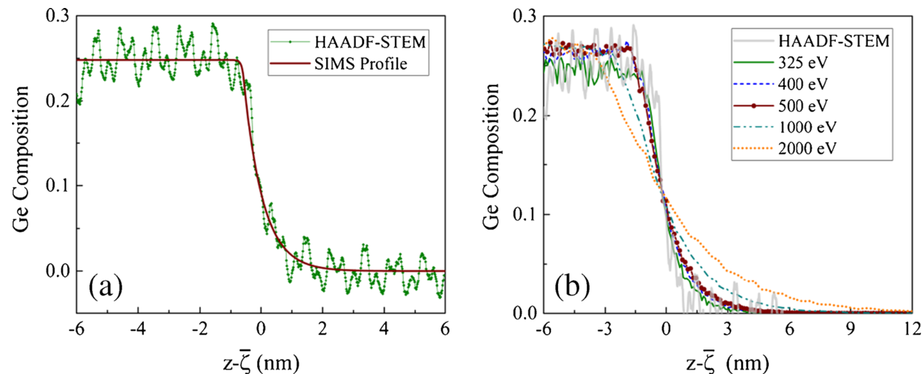

Figure 6. (Color on-line) **(a)** Comparison of the interface measured by HAADF-STEM and by simultaneous fitting of the SIMS profiles. The SIMS profile has not been scaled. **(b)** Comparison of the interface profile determined from HAADF-STEM and SIMS depth profiles at selected energies. The data has been rescaled such that the profiles overlie at the expectation point of the fitted functions allowing direct comparison between the data sets

energies. The parameter determination becomes inaccurate only when energies above 400 eV are used in the global fit, limited in our case both by the number of profiles remaining and the lack of data from sufficiently low enough energies where the broadening is low.

The approach we have adopted allows quantitative SIMS analysis of interfaces to be performed. Our choice of (a) interface model and (b) SIMS resolution function, are somewhat arbitrary and potentially overly-simplified. Different functions could be adopted to replace Equations 2 and/or 5. Sample models based on symmetrical or asymmetrical error functions, for example, would be an obvious choice if the interface profile were a result of solid state diffusion. Our choices, however, ensured that the convolution function was not overly complex and minimized the number of fit parameters and, hence, energy profiles required. Other, more physically realistic choices for Equations 2 and 5 would result in more complex convolved functions. Ultimately, the quality of the data, and the number of energy profiles required to meet the fitting criteria, are the limiting factors in differentiating between various models [25].

Our fitting methodology does, however, enable the shape of a SiGe/Si interface to be determined using energy sequencing. Moreover, we have demonstrated that buried interfaces can be determined to sub-nanometer precision using ion beam energies readily available in modern SIMS instruments if the (energy-dependent) matrix effect can be accounted for (i.e., the profiles can be linearized). It is, perhaps, surprising that the same interface profile can be obtained from two techniques that analyze the sample over very different length scales (square microns for SIMS and a couple of nanometers for TEM). Rough surfaces with many terraces and pits may cause additional blurring in the SIMS profile. However, the SIMS linear gate size of only 6.25% means that ions are only collected from the central ~13.8×13.8 μm of the crater region. This area is of a similar order to that of the AFM measurements in which we did not observe significant surface features. However, AFM measures the native oxide, which could potentially mask some surface topography, although the presence of a large number of atomic steps seems unlikely. Nevertheless, some atomic steps are inevitable over a 200 μm^2 area, but as the incident beam is normal to the surface, and therefore parallel to the steps, their effect on the SIMS profile appears to be limited. For very rough surfaces, a more complicated metrology would need to be developed. However, the metrology approach developed and demonstrated herein extends the current capabilities of SIMS analyses allowing the spatial extent of interfaces in well-behaved materials to be determined accurately and with minimal sample preparation. The metrology is easily extended to other material systems and would be able to quantify interfaces sharper than that reported here.

Conclusions

uleSIMS using an O_2^+ primary beam and energy sequencing from 0.25 to 2.5 keV has been used to obtain a quantitative profile from a $Si_{0.73}Ge_{0.27}$/Si interface, with uncertainties on the profile shape in the sub-nanometer range. The simple approach adopted here uses the convolution of two parameterized functions chosen to ensure that a wide range of interface profiles from well-behaved materials can be modeled. Given the interdependency between the intrinsic sample and energy-dependent SIMS parameters, simultaneous fitting was applied to determine the sample parameters using a simplistic SIMS response function. The resulting interface parameters were found to be in excellent agreement with those determined independently from the HAADF-STEM data measured from the same sample.

References

1. Morris, R.J.H., Grasby, T.J., Hammond, R., Myronov, M., Mironov, O.A., Leadley, D.R., Whall, T.W., Parker, E.H.C., Currie, T.W., Leitz, C.W., Fitzgerald, E.A.: High conductance Ge p-channel heterostructures realized by hybrid epitaxial growth. Semicond. Sci. Technol. **19**, L1–L4 (2004)
2. International Technology Roadmap for Semiconductors (2013). http://www.itrs2.net/
3. Morris, R.J.H., Dowsett, M.G., Beanland, R., Dobbie, A., Myronov, M., Leadley, D.R.: Overcoming Low Ge Ionization and Erosion Rate Variation for Quantitative Ultralow Energy Secondary Ion Mass Spectrometry Depth Profiles of $Si_{1-x}Ge_x$/Ge Quantum Well Structures. Anal. Chem. **84**, 2292–2298 (2012)
4. Wittmaack, K., Wach, W.: Profile distortions and atomic mixing in SIMS analysis using oxygen primary ions. Nucl. Inst. Methods **191**, 327–334 (1981)
5. Clegg, J.B.: Depth profiling of shallow Arsenic implants in Silicon using SIMS. Surf. Interface Anal. **10**, 332–337 (1987)
6. Dowsett, M.G., Chu, D.P.: Quantification of secondary-ion-mass spectroscopy depth profiles using maximum entropy deconvolution with a sample independent response function. J. Vac. Sci. Technol. B **16**(1), 377–381 (1998)
7. Clegg, J.B., Smith, N.S., Dowsett, M.G., Theunissen, M.J.J., de Boer, W.B.: Secondary ion mass spectroscopy resolution with ultra-low beam energies. J. Vac. Sci. Technol. A **14**(4), 2645–2650 (1996)
8. Deline, V.R., Katz, W., Evans Jr., C.A., Williams, P.: Mechanism of the SIMS matrix effect. Appl. Phys. Lett. **33**, 832–835 (1978)
9. Gillen, G., Phelps, J.M., Nelson, R.W., Williams, P., Hues, S.M.: Secondary ion yield matrix effects in SIMS depth profiles of Si/Ge multilayers. Surf. Interface. Anal. **14**, 771–780 (1989)
10. Anderson, H.H.: The depth resolution of sputter profiling. Appl. Phys. **18**, 131–140 (1979)
11. Morris, R.J.H., Dowsett, M.G.: Ion yields and erosion rates for $Si_{1-x}Ge_x$ ($0 \leq x \leq 1$) ultralow energy O_2^+ secondary ion mass spectrometry in the energy range of 0.25–1 keV. J. Appl. Phys. **105**(9), 114316 (2009)
12. Dowsett, M.G., Morris, R., Chou, P.-F., Corcoran, S.F., Kheyrandish, H., Cooke, G.A., Maul, J.L., Patel, S.B.: Charge compensation using optical conductivity enhancement and simple analytical protocols for SIMS of resistive $Si_{1-x}Ge_x$ alloy layers. Appl. Surf. Sci. **203/204**, 500–503 (2003)
13. Kirkland, E.J., Loane, R.F., Silcox, J.: Simulation of annular dark field STEM images using a modified multislice method. Ultramicroscopy **23**, 77–96 (1987)
14. Voyles, P.M., Muller, D.A., Grazul, J.L., Citrin, P.H., Gossmann, H.-J.L.: Atomic-scale imaging of individual dopant atoms and clusters in highly *n*-type bulk Si. Nature **416**, 826–829 (2002)
15. Paul, D.J.: Si/SiGe heterostructures: from material and physics to devices and circuits. Semicond. Sci. Technol. **19**, R75–R108 (2004)
16. Jiang, Z.X., Kim, K., Lerma, J., Corbett, A., Sieloff, D., Kottke, M., Gregory, R., Schauer, S.: Quantitative SIMS analysis of SiGe

composition with low energy O_2^+ beams. Appl. Surf. Sci. **252**, 7262 (2006)

17. Sobers Jr., R.C., Franzreb, K., Williams, P.: Quantitative measurement of O/Si ratios in oxygen-sputtered silicon using ^{18}O implant standards. Appl. Surf. Sci. **231/232**, 729–733 (2004)
18. Huyghebaert, C., Conard, T., Brijs, B., Vandervorst, W.: Impact of the Ge concentration on the Ge-ionization probability and the matrix sputter yield for a siGe matrix under oxygen irradiation. Appl. Surf. Sci. **231/232**, 708–712 (2004)
19. Vandervorst, W., Janssens, T., Huyghebaert, C., Berghmans, B.: The fate of the (reactive) primary ion: sputtering and desorption. Appl. Surf. Sci. **255**, 1206–1214 (2008)
20. Reuter, W.: A SIMS XPS Study on Silicon and Germanium under O_2^+ Bombardment. Nucl. Inst. Methods B **15**, 173–175 (1986)
21. Dowsett, M.G., Barlow, R.D., Allen, P.N.: Secondary ion mass spectrometry analysis of ultrathin impurity layers in semiconductors and their use in quantification, instrumental assessment, and fundamental measurements. J. Vac. Sci. Technol. B **12**(1), 186–198 (1994)
22. Zalm, P.C., de Kruif, R.C.M.: Problems in the deconvolution of SIMS depth profiles using delta-doped test structures. Appl. Surf. Sci. **70/71**, 73–78 (1993)
23. Dowsett, M.G., Rowlands, G., Allen, P.N., Barlow, R.D.: An analytic form for the SIMS response function measured from ultra-thin impurity layers. Surf. Interface Anal. **21**, 310–315 (1994)
24. Dowsett, M.G., Barlow, R.D.: Characterization of sharp interfaces and delta doped layers in semiconductors using secondary ion mass spectrometry. Anal. Chim. Acta **297**, 53–275 (1994)
25. Hughes, I.G., Hase, T.P.A.: Measurements and their uncertainties, pp. 67–82. Oxford University Press, Oxford, UK (2010)
26. Dowsett, M.G.: Depth resolution parameters and separability. In: Benninghoven, A., Hagenhoff, B., Werner, H.W. (eds.) Secondary Ion Mass Spectrometry X. P. 355. Wiley, Chichester, UK (1997)